ACS APPLIED MATERIALS & INTERFACES

Research Article

www.acsami.org

Preparation and Characterizations of Bioglass Ceramic Cement/Ca−P Coating on Pure Magnesium for Biomedical Applications

Xue Zhang,[†,‡] Xiao-Wu Li,[*,†,‡] Ji-Guang Li,[‡] and Xu-Dong Sun[‡]

[†]Institute of Materials Physics and Chemistry, College of Sciences, Northeastern University, Shenyang 110819, P. R. China

[‡]Key Laboratory for Anisotropy and Texture Engineering of Materials, Ministry of Education, Northeastern University, Shenyang 110819, P. R. China

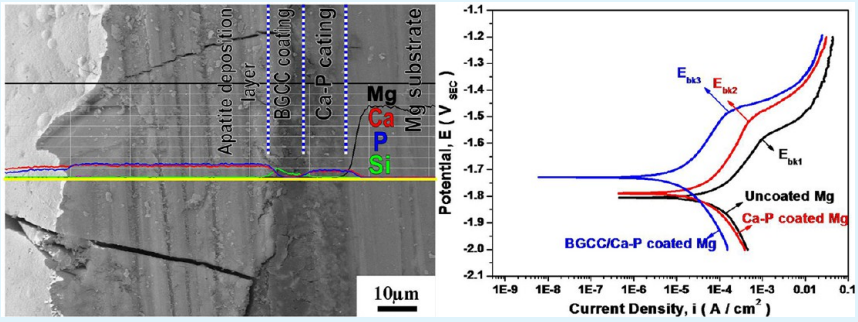

ABSTRACT: Magnesium has been recently recognized as a biodegradable metal for bone substitute applications. In order to improve the biocompatibility and osteointegration of pure Mg, two kinds of coatings, i.e., the Ca−P coating and bioglass ceramic cement (BGCC)/Ca−P coating, were prepared on the pure Mg ribbons in the present work. The Ca−P coating was obtained by aqueous solution method. Subsequently, Ca−P coated Mg was immersed into the BGCC slurry, which was prepared by the mix of SiO_2−CaO−P_2O_5 bioglass ceramic (BGC) powders and phosphate liquid with a liquid-to-solid ratio (L/S) of 1.6, to obtain BGCC/Ca−P coating by a dipping−pulling method. The microstructures, morphologies, and compositions of these coatings have been characterized by X-ray diffraction (XRD) and scanning electron microscopy (SEM) with energy-dispersive spectroscopy (EDS). The effect of these coatings on the mineralization activity of pure Mg has been investigated. The results indicated that both the Ca−P coating and BGCC/Ca−P coating could promote the nucleation of osteoconductive minerals, i.e., bone-like apatite, and the hydroxyapatite (HA) layer formed on the surface of the BGCC/Ca−P coating is obviously more dense, thick, and stable than that formed on the Ca−P coating after immersion in SBF solution for 15 days. The potentiodynamic polarization test indicated that the corrosion current density of the BGCC/Ca−P coated Mg is obviously lower than that of the Ca−P coating and 10 times lower than that of uncoated Mg. These results demonstrated that the BGCC/Ca−P coating can increase significantly the corrosion resistance of Mg and introduce a high biocompatibility of the bone−Mg substrate interface. In summary, the newly developed BGCC/Ca−P coated Mg has a good potential for biomedical applications.

KEYWORDS: *coating, magnesium, BGCC, Ca−P, mineralization, corrosion*

1. INTRODUCTION

Magnesium and its alloys have recently received much attention as one of the potential biodegradable bone implant materials due to their advantageous performances, such as a density comparable with that of human bone, excellent biodegradability, biocompatibility, and bioresorbability,[1−5] a relatively low elastic modulus matchable with human bone, etc. Moreover, Mg is essential to human metabolism and is naturally found in bone tissue. However, the rapid corrosion of magnesium and its alloys in chloride containing solutions including human body fluid or plasma has limited their clinical applications.[6,7] Meanwhile, hydrogen gas could yield collectively around the Mg implants as a result of fast corrosion.[2] Therefore, it is very important to improve the corrosion resistance of Mg and its alloys in order that they can be applied clinically. In recent years, there have been some methods available for improving the corrosion resistance of Mg, for example, Mn and Zn[8−11] as well as Ca[12−14] were used as alloying elements for enhancing efficiently the corrosion resistance of magnesium alloys.

Although the element alloying can increase the bio-corrosion resistance of Mg to some extent, alloying cannot significantly improve the bone response to magnesium alloys, especially at the early stage of implantation. Thus, it is also necessary to find the efficacious surface modification technologies for reducing the degradation rate and introducing a highly biocompatible bone−implant interface. Coatings of osteoconductive minerals, e.g., hydroxyapatite ($Ca_{10}(PO_4)_6(OH)_2$, HA) and tricalcium phosphate (Ca_3PO_4, TCP), have been often used for improving the biocompatibility of biomedical metals, since such coatings

Received: October 17, 2013
Accepted: December 2, 2013
Published: December 2, 2013

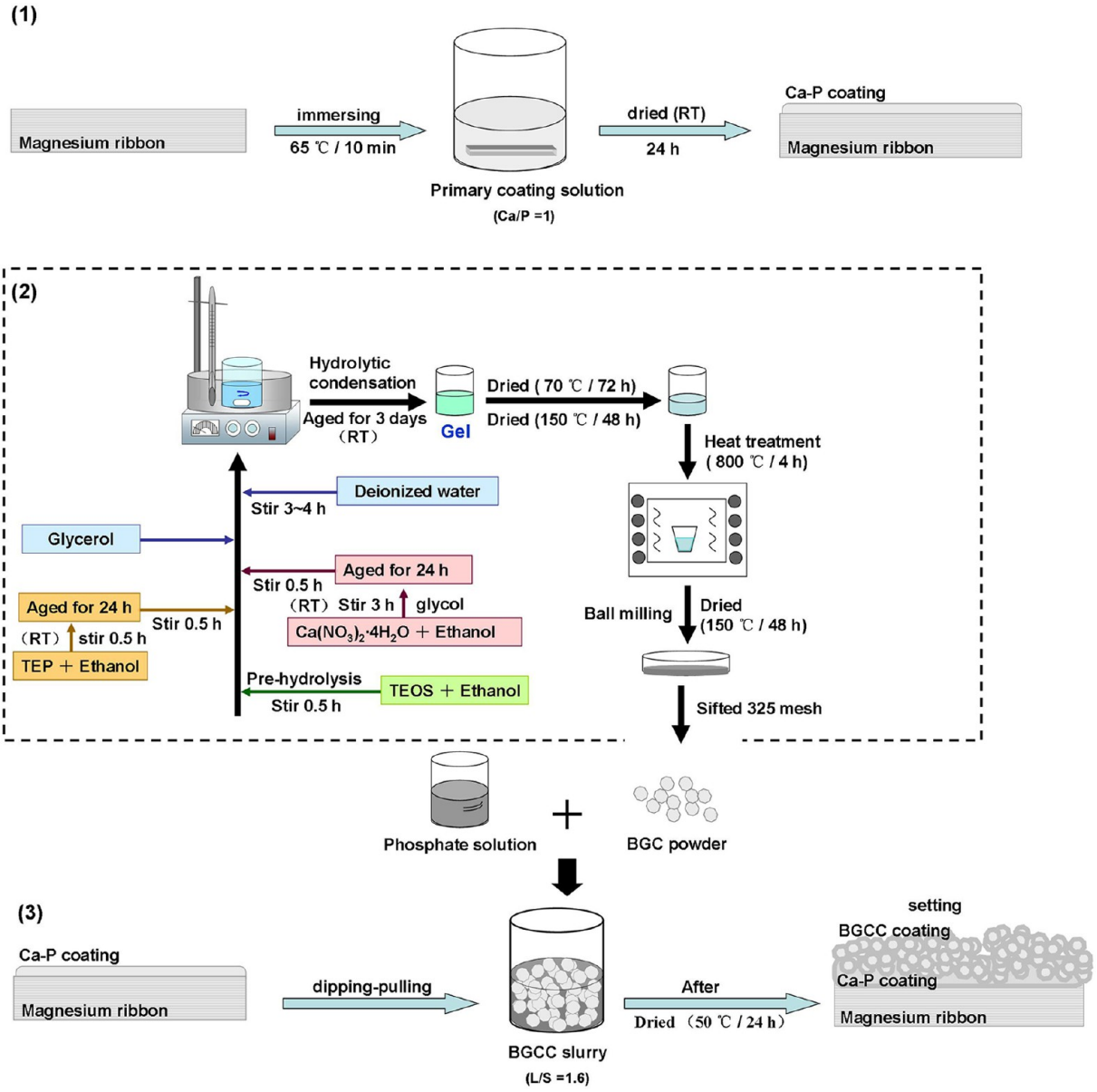

Figure 1. Schematic illustration of the processing steps for (1) as-primary Ca−P coated Mg, (2) the fabrication of the BGC powders, and (3) BGCC coating on the surface of Ca−P coated Mg.

can promote the new bone growth and osteointegration around metal implants.

Currently available methods for producing various Ca−P coatings on magnesium mainly include an aqueous solution method and an electrodeposition method. Through the aqueous solution method, osteoconductive minerals, mainly including dicalcium phosphate dihydrate ($CaHPO_4{\cdot}2H_2O$, DCPD), HA, and octacalcium phosphate ($Ca_8H(PO_4)_6{\cdot}5H_2O$, OCP), are directly deposited on the substrate surface of Mg and its alloys.[15−20] For instance, Cui et al.[15] reported that Ca−P coating was formed on the surface of AZ31 Mg alloys by immersing the alloy samples in the supersaturated calcification solution. Hiromoto and Yamamoto[16] developed a new method for the direct synthesis of HA on magnesium using a Ca chelate compound and found that a sufficiently high concentration of Ca ions on the magnesium surface could overcome the prevention of HA crystallization with Mg ions. Xu et al.[17,18] reported that the DCPD deposition layer prepared on Mg alloys in a phosphate solution could be transformed into HA during the immersion in SBF solution and that cells L929 showed good adherence, high growth rate, and proliferation characteristics on the Ca−P coated magnesium alloy in in vitro cell experiments. Meanwhile, their in vivo experiments demonstrated that the Ca−P coating provided magnesium with a significantly good surface bioactivity and promoted early bone growth at the implant/bone interface. Chen et al.[19] selected the composition of the coating solution according to an equilibrium thermodynamic diagram of calcium phosphates calculated using MEDUSA software,[20] and they found that a secondary/post-treatment in alkaline solution was crucial for generating a HA component within the coating upon Mg.

Electrochemical deposition was recently employed by some investigators as the other technique to form DCPD or HA upon Mg alloys for the purposes of degradation control.[21−24] Song et al.[21] found that the as-electrodeposited coating on AZ91D Mg alloys consisting of DCPD and β-tricalcium

dx.doi.org/10.1021/am404574t | ACS Appl. Mater. Interfaces 2014, 6, 513−525

Table 1. Ion Concentrations and pH of the SBF Solution and Human Blood Plasma (units: mM)[30]

	Na^+	K^+	Mg^{2+}	Ca^{2+}	Cl^-	HCO_3^{2-}	HPO_4^{2-}	SO_4^{2-}	pH
SBF	142.0	5.0	1.5	2.5	148.8	4.2	1.0	0.5	7.40
HBP	142.0	5.0	1.5	2.5	103.0	27.0	1.0	0.5	7.20−7.40

phosphate (β-TCP) was transformed to uniform HA after alkali heat treatment. Wen et al.[22] and Meng et al.[23] successfully prepared the fluoride doped HA (FHA) coating on Mg alloys through the addition of 40% HF solution (toxic) in the pretreatment process, and they found that the coating was protective against corrosion in SBF solution. Song et al.[24] also reported that both the HA and the FHA coatings on Mg alloys could promote the nucleation of osteoconductive minerals, i.e., bone-like apatite or β-TCP, after immersion in SBF solution for 1 month. However, the HA coating transformed from DCPD through an alkali heat treatment was fragile and less stable, and therefore its long-term corrosion resistance cannot be assured.

Quite recently, a microarc oxidation (MAO) process was introduced by Wang et al.[25] to fabricate dense oxide coatings formed in alkaline silicate electrolyte with and without titania sol addition on Mg alloys. They found that the coating prepared by the MAO method on AZ91 Mg alloys could slow down the biodegradation rate, to some extent, after a long-term immersion in SBF solution. However, the microarc oxidation layer prepared by the MAO method cannot improve the bone response to magnesium alloys. Afterwards, Wu et al.[26] fabricated four calcium phosphate/chitosan composite coatings on the surface of micro-arc oxidized AZ91 Mg alloy through electrophoretic deposition. Liu et al.[27] and Tang et al.[28] prepared DCPD or HA coating on the surface of micro-arc oxidized pure Mg and AZ31 Mg alloys through the aqueous solution method, by using the MAO layer as an anticorrosive transition layer, and by this way, the corrosion resistance and bioactivity of these MAO and Ca−P two-layer coatings have been concurrently improved.

In order to find out a more efficient surface modification technology for reducing the degradation rate and introducing a high biocompatibility of the bone−Mg substrate interface, in the present work, an aqueous solution method was employed, for the first step, to form an intermediate transition layer, i.e., a Ca−P coating, on the surface of the pure Mg substrate, and subsequently, a novel SiO_2−CaO−P_2O_5 bioglass ceramic cement (BGCC) coating was synthesized on the surface of Ca−P coated Mg by a dipping−pulling method. It should be mentioned here that, since chemical properties of pure Mg are much more active than those of other Mg alloys (e.g., AZ91, AZ31), pure Mg was selected as the substrate in the present work in order to noticeably highlight the protective function of the BGCC/Ca−P coating to the substrate by in vitro degradation tests and corrosion tests. Actually, bioglass cement (BGC) material was firstly prepared by Kokubo et al.,[29] who reported that the glass powder would become hardened when mixed with a phosphate solution to form BGC, which was then transformed to HA after being immersed in SBF solution for 3 days. Drawing inspiration of Kokubo's work,[29] a new BGCC slurry was used in the present work for the preparation of the coating on the Ca−P coated Mg to promote the nucleation of osteoconductive minerals. The microstructure and composition of the coating were investigated, and the degradation behavior was examined by electrochemical and immersion tests in terms of mineralization.

2. MATERIALS AND METHODS

2.1. Sample Preparation. The commercially pure magnesium ribbons (purity: 99.9%) with a dimension of 8 mm × 4 mm × 0.3 mm were used as substrate materials. After these ribbon samples were ultrasonically cleaned in ethanol for 5 min and dried in warm air, they were first immersed in a mixed alkaline solution of Na_3PO_4 (50-80 g/L) and NaOH (30−37 g/L) at 70 °C for 8 min for degreasing and subsequently immersed in an acid solution (75 wt %) of H_3PO_4 at room temperature (RT) for 30 s for surface activation.

2.2. Synthesis of Bioactive BGCC/Ca−P Coatings. In the present work, the conversion coating process requires two steps described as follows:

(1) Synthesis of a Transition Layer of Ca−P Coating. The primary coating solution contains 0.01 M $Ca(NO_3)_2{\cdot}4H_2O$ and 0.01 M Na_3PO_4 along with 1.00 g/L H_3PO_4, which was added into the solution to adjust the pH value to 4.5. The primary coating process was thus conducted by immersing Mg ribbons into the coating solution at 65 °C for 10 min to obtain a Ca−P coating on the surface of ribbons and then dried at RT for 24 h (see Figure 1(1)).

(2) Synthesis of BGCC Coating. A gel glass with nominal composition of 0.54 SiO_2, 0.40 CaO, and 0.06 P_2O_5 (mol %) was synthesized by hydrolysis and polycondensation of tetraethoxysilane ($Si(OC_2H_5)_4$, TEOS), calcium nitrate tetrahydrate ($Ca(NO_3)_2{\cdot}4H_2O$), and tri-ethyl phosphate ($OP(OC_2H_5)_3$, TEP), with ethanol being used as a solvent and nitric acid (HNO_3) as catalyst. Specifically, in the course of preparation, 5.46 g of TEP were dissolved in 15 mL of ethanol and gently stirred at RT for 0.5 h; 23.6 g of $Ca(NO_3)_2{\cdot}4H_2O$ were in 50 mL of ethanol and gently stirred at RT for 4 h; and both kinds of solutions were then aged for 24 h. A total of 28.08 g of TEOS were dissolved into 40 mL of ethanol. After stirring for 0.5 h, TEP and $Ca(NO_3)_2{\cdot}4H_2O$ were in turn added to the TEOS solution, and the mixture was stirred again for 0.5 h, respectively. Then a little glycerol and deionized water were added to the mixture to promote the reaction of hydrolysis−polycondensation. The solution was aged for 3 days until gelation occurred, and the gels were further dried at 70 °C for 24 h and at 150 °C for 24 h and finally heat-treated at 800 °C for 4 h in air for obtaining the bioglass ceramic (BGC). The BGC was mixed in a ball mill together with ZrO_2 balls and ethanol. After sufficient mixing, the BGC powders were dried at 150 °C for 48 h and sifted through a 325 mesh sieve to obtain the final glass powders with the size less than 45 μm. Figure 1(2) shows clearly the detailed processing steps for producing glass powders. A total of 12.0 g of $(NH_4)_2HPO_4$ and 0.1 g of $Ca(H_2PO_4)_2$ were dissolved into 50 mL of deionized water to form a phosphate solution with pH = 7.64. The prepared BGC powders and the phosphate liquid with a liquid-to-solid ratio (L/S) of 1.6 were mixed in a 96 holes cell culture plate to form BGCC slurry. Following this, as-primary Ca−P coated Mg was immersed into the BGCC slurry at a dipping/pulling speed of 1.6 mm/s, and the top surface was coated with one layer of BGCC coating at RT (see Figure 1(3)). Finally, the BGCC/Ca−P coated Mg were dried at 50 °C for 24 h and kept in a desiccator for further characterizations.

2.3. Evaluation of in Vitro Degradation. Each Mg, Ca−P coated Mg, and BGCC/Ca−P coated Mg specimen was molded into epoxy resin with only one side (i.e., top surface) being exposed. These specimens were immersed in SBF solution to evaluate their in vitro degradation behavior. The specimens were soaked into 50 mL of SBF at temperatures of 36.5 ± 0.5 °C for 3, 5, 7, 15, and 30 days, respectively. The ion concentrations of the SBF solution are quite similar to that of human blood plasma (Table 1).[30] After immersion, the specimens were washed with deionized water and dried at RT for 48 h.

The phase composition of the Mg with and without coatings was evaluated by X-ray diffraction (XRD) and energy dispersive X-ray spectrometer (EDS) in a scanning electron microscope (SEM), respectively. The XRD data were obtained over the 2θ range of 20–60° at a step size of 0.25°. The surface morphologies of the Mg with and without coatings before and after being soaked in SBF solution were examined using the SSX-550 SEM. The changes of ion concentrations and pH values in SBF as a function of soaking time were measured using the 4300DV inductively coupled plasma–atomic emission spectrometry (ICP-AES) and the PHS-3E pH meter, respectively.

2.4. Corrosion Tests. Electrochemical tests were carried out in SBF solution with pH of 7.4 at 37 °C to measure the corrosion rate. The area of the working electrode was 3.5 mm × 3.8 mm. Potentiodynamic polarization (PDP) was performed. A three electrode setup was used with a Pt counter electrode and a saturated calomel reference electrode. PDP tests were carried out after 20 min in solution to allow the open circuit potential to stabilize. A scan rate of 1 mV/s was utilized in PDP tests.

3. RESULTS AND DISCUSSION

3.1. Phase Compositions, Morphologies, and Microstructures of Ca–P Coating and BGCC/Ca–P Coating. Figure 2 shows the XRD patterns of the Mg and Ca–P coated

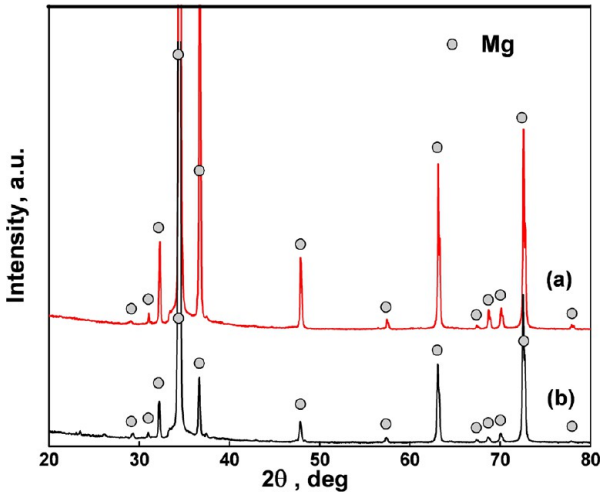

Figure 2. XRD patterns of Mg (a) and Ca–P coated Mg (b).

Mg. There is no clear change in the XRD results of the Ca–P coating on Mg (Figure 2a) as compared to the typical diffraction peaks of pure Mg (Figure 2b).

Figure 3 shows the XRD patterns of the BGC powder, BGCC slurry, and BGCC/Ca–P coated Mg. It should be pointed out that the sample of BGCC slurry for XRD tests is in a solidified state. From Figure 3a one can see that the crystalline phase compositions of the synthesized BGC powders are mainly composed of $Ca_2SiO_4{\cdot}0.05Ca_3(PO_4)_2$ and $Ca_2P_2O_7$. With matching the diffraction peaks of BGCC slurry (Figure 3b), there are some relevant broadened peaks (except for those peaks coming from Mg) of the surface of BGCC/Ca–P coating (Figure 3c), the phase compositions of which consist mainly of calcium deficient hydroxyapatite ($Ca_9HPO_4(PO_4)_5OH$, CDHA).

Figure 4 shows the surface morphologies of Ca–P coating, BGCC coating, and the cross-section of the BGCC/Ca–P coated Mg. From Figure 4a it seems that the surface of the Mg substrate is not uniformly covered with Ca–P coatings; however, the EDS collected upon the surface of the Ca–P

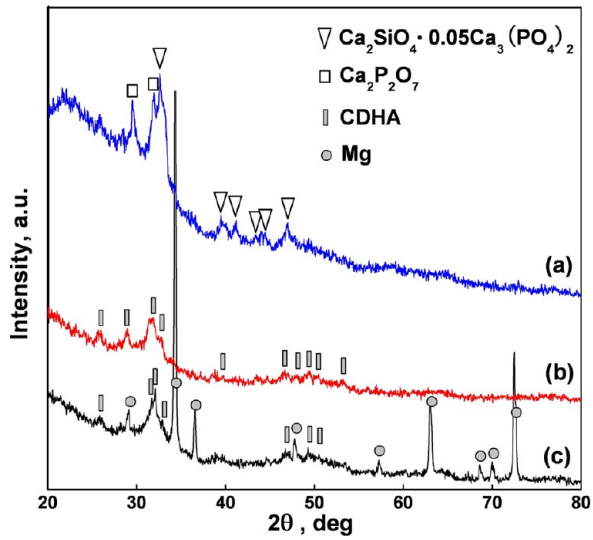

Figure 3. XRD patterns of BGC powder (a), BGCC slurry (b), and BGCC/Ca–P coated on Mg (c). (Note: CDHA: calcium defficient hydroxyapatite, $Ca_9HPO_4(PO_4)_5OH$).

coating shows that the coating comprises C, O, Mg, P, and Ca elements (see Figure 4b), indicating that there should be a thin Ca–P coating closely adhesive to the surface of the Mg substrate. Since the Ca–P coating is too thin, the Mg beneath the coating leads to a strong Mg signal, which dominates the XRD (Figure 2b) and EDS spectra (Figure 4b). This phenomenon may be attributed to a short immersion time (10 min) and a slow precipitation rate of Ca–P coating on the surface of Mg substrate during the first coating step. Meanwhile, there are two kinds of external crystals irregularly forming on the top surface of the Ca–P coating: one is featured by broccoli-like structure several micrometers in size, and its Ca/P molar ratio is approximately 1.00; the other one has a feather-like morphology with a regular shape. As indicated in the work by Chen et al.,[19] HNO_3 was used to adjust the pH value of the same coating solution, and the formed Ca–P coating consisted of precipitated sub-micrometer flakes. Since H_3PO_4, rather than HNO_3, was used to adjust the pH value of the primary coating solution in the present work, the phosphate ion concentration of the solution is higher than that of the work by Chen et al.,[19] and the Ca/P molar ratio of the inner layer of the Ca–P coating is lower than 1.00. This should be the major reason why different morphologies of crystals were formed on the pure Mg substrate in the present work and the work by Chen et al.[19]

From Figure 4c, it can be seen that there are two different sizes of particles on the surface of the BGCC coating after setting at 50 °C for 24 h and that there are some cracks around the large particles, resulting from the consuming of phosphate solution during the setting process and the lower adhesive strength between the large and small particles. The EDS analysis data of those two kinds of particles are listed in Table 2. The Ca/P molar ratio of the large particle is slightly higher than 1.00, and its size ranges roughly from 5 to 20 μm. In contrast, the Ca/P molar ratio of the small particle is slightly higher than 2.00, and its particle size is approximately in the range of sub-micrometer. The inner layer of the BGCC coating has a Ca/P molar ratio of 1.55 (see Figure 4d).

During the process of the secondary coating step, the adopted BGCC slurry is a mixture of BGC powders and

dx.doi.org/10.1021/am404574t | ACS Appl. Mater. Interfaces 2014, 6, 513–525

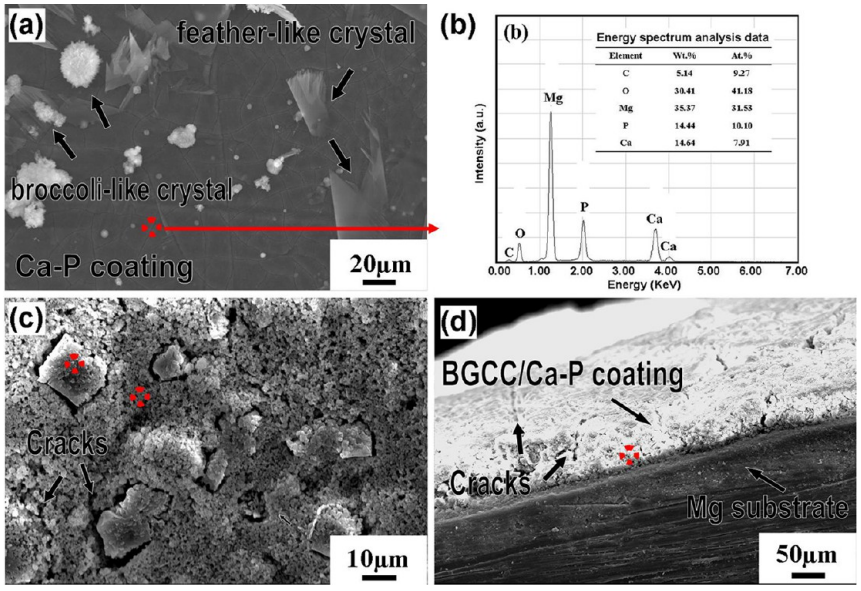

Figure 4. SEM images showing the surface morphologies of Ca–P coated Mg (a), with relevant EDS spectra of the surface of the Ca–P coated Mg (b), BGCC coating (c), and cross-section of the BGCC/Ca–P coated Mg (d). (The point sites of the EDS.)

Table 2. EDS Analysis Data of the BGCC/Ca–P Coating

BGCC coating		Si		Ca		P		O		Ca/P molar
		wt %	atom %	wt %	atom %	wt %	atom %	wt %	atom %	
Surface (Figure 4c)	large particle	7.91	6.03	25.79	13.78	18.54	12.82	40.02	53.56	1.07
	small particle	19.79	14.62	21.63	11.19	7.84	5.25	43.45	56.34	2.13
inner layer (cross section, Figure 4d)		23.21	17.75	18.43	9.87	9.18	6.37	49.18	66.01	1.55

Table 3. Comparisons of the Preparation of BGC and BGCC by Different Processing Routes

materials	cement powder	phosphate solution	L/S ratio	pH value	soaked in SBF	reference
BGC	$CaO–SiO_2–P_2O_5–CaF_2$ (BG)	$(NH_4)_2HPO_4$ $NH_4H_2PO_4$	0.5	7.4	HA	29
BGC	$CaO–SiO_2–P_2O_5$ (BG)	$(NH_4)_2HPO_4$ $NH_4H_2PO_4$	0.45	7.0	HA	31
BGC	$CaO–SiO_2–P_2O_5–MgO–CaF_2$ (BG)	$H_3C_6H_5O_7$	0.8	–	$CaPO_3F$	32
		Na_2HPO_4		–	$CaSiO_3$	
		$H_3C_6H_5O_7$	0.35	–	HA	
		K_2HPO_4 KH_2PO_4		–		
BGCC	$CaO–SiO_2–P_2O_5$ (BGC)	$(NH_4)_2HPO_4$ $Ca(H_2PO_4)_2$	1.6	7.64	HA	present work

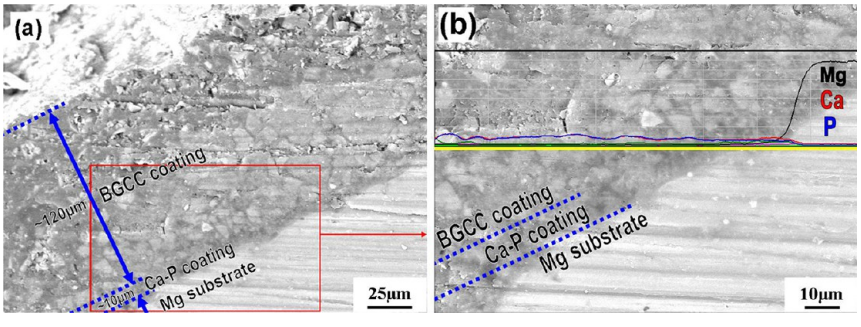

Figure 5. BSE images of the cross-section (a) and corresponding distribution of Mg, Ca, and P on this section (b) of the BGCC/Ca–P coated Mg. The line scan was performed along the yellow line in (b).

phosphate solution ($(NH_4)_2HPO_4$ and $Ca(H_2PO_4)_2$), and the L/S ratio was chosen as 1.6, which is much higher than the traditional L/S ratio (L/S < 1.0) (see Table 3). When the L/S ratio is lower than 1.0, the mixture appears in a white paste

dx.doi.org/10.1021/am404574t | ACS Appl. Mater. Interfaces 2014, 6, 513–525

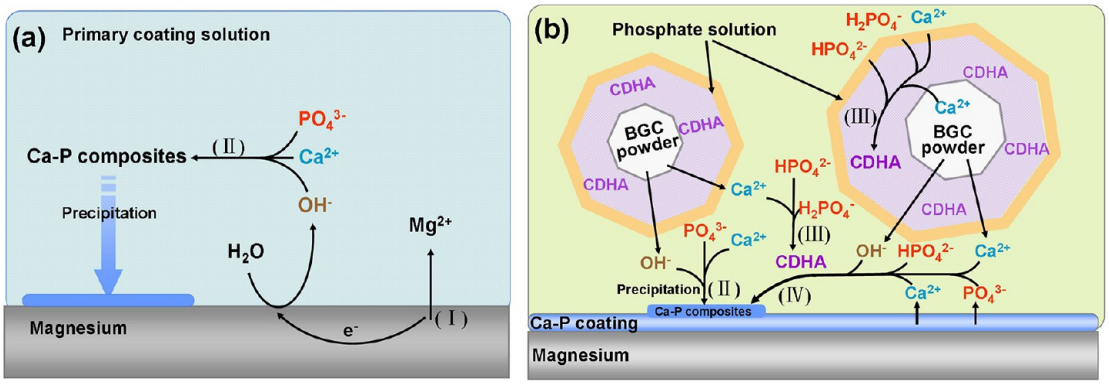

Figure 6. Schematic illustrations showing the deposition mechanisms of Ca–P coating (a) and BGCC/Ca–P coating (b) on Mg substrate in coating solutions.

state. In contrast, the mixture presents in a white slurry state in the present work. Liu et al.[32] has reported that the setting time should increase as the L/S ratio increases. Thus, the slurry state can last for extended periods during coating process as a result of a higher L/S ratio of 1.6 for the mixture, and this state of the mixture, i.e., BGCC coating slurry, is conducive not only to a greater uniformity of BGCC coating on the Ca–P coated Mg but also to a further enhancement of the bonding strength between BGCC and Ca–P coatings.

The back scatter electron (BSE) image of the distribution of Mg, Ca, and P elements on the cross-section of the BGCC/Ca–P coated Mg is shown in Figure 5. The different coating layers can be clearly seen, and the thicknesses of the Ca–P coating and BGCC/Ca–P coating were measured to be ~10 μm and ~120 μm, respectively (Figure 5a). In a magnified image of Figure 5b, it can be seen that the interface is not so obvious between the BGCC coating and Ca–P coating, and the line scan profiles of Ca and P elements almost keep unchanged across the Ca–P and BGCC coating layers. Moreover, Ca and P elements were also detected in the region of the Mg substrate, which is near the interface of Ca–P coating and Mg substrate. These results indicate that the Ca–P coating could act as an effective intermediate transition layer, which has tight bonding interfaces both with Mg substrate and outer BGCC coating. Meanwhile, the mutual diffusion of elements has occurred in different layers, i.e., the Mg substrate, the intermediate transition layer of Ca–P coating, and the outer layer of BGCC coating.

3.2. Precipitation Mechanism of Ca–P Coating and BGCC/Ca–P Coatings. The formation of Ca–P composites on the metal substrate by the aqueous solution method depends on the Ca/P molar ratio, temperature, local pH value, etc.[15,33,34] However, since Mg is more reactive and corrosive than other biometals and the excess Mg ions prevent HA crystallization, it is difficult to fabricate directly HA on the surface of Mg substrate.[35] In order to activate the nucleation of apatite on Mg, two different methods have been used in the present work.

Figure 6 gives schematically the process where the Ca–P coating and BGCC/Ca–P coating are deposited on Mg substrate in the primary coating solution and the BGCC slurry, respectively. The following reactions are suggested to account for the formation of the Ca–P coating and BGCC/Ca–P coating:

(I) Since Mg is "active" at low pH, Mg ions (Mg^{2+}) are released from the Mg substrate into the primary coating solution and hydrogen (H_2) gas is produced (see Figure 6a,I):

$$Mg + 2H_2O \rightarrow Mg^{2+} + 2OH^- + H_2\uparrow \quad (1)$$

(II) In the primary coating solution with a pH value of 4.5, the pH value on the surface is steeply elevated with rapid corrosion of Mg. In the acidic environment, the above reactions occur at high rates, and the accumulation of hydroxyl ions (OH^-) can increase the pH value at the local surface of Mg substrate. Meanwhile, there are a lot of calcium ions (Ca^{2+}) and phosphate ions (PO_4^{3-}), which are provided from the primary coating solution. Thus, the pH value on the local surface increases, leading to the formation and the precipitation of Ca–P composites upon the Mg substrate (see Figure 6a,II), according to the following equation:

$$PO_4^{3-}(\text{excess}) + Ca^{2+} + OH^- \rightarrow \text{Ca–P composites}$$
$$(\text{The molar ratio of Ca/P} < 1) \quad (2)$$

(III) After Ca–P composite coated Mg was dried at RT for 24 h, the BGCC coating was further produced on it in a BGCC slurry by a dipping–pulling method at RT, and the schematic illustration of the relevant forming process is given in Figure 6b. Seeing from the XRD result (Figure 3a), the BGC powders are mainly composed of $Ca_2SiO_4{\cdot}0.05Ca_3(PO_4)_2$, and Ca_2SiO_4 is one of the main constituents in ordinary Portland cement and can spontaneously develop strength toward water.[36,37] Fujii and Konda[38] reported that $CaO{\cdot}SiO_2{\cdot}H_2O$ and $Ca(OH)_2$ are the hydration products of Ca_2SiO_4 at 20 °C and the following hydration formula occurs:

$$\beta\text{-}Ca_2SiO_4 + 2.61H_2O \rightarrow 1.80CaO{\cdot}SiO_2{\cdot}2.41H_2O + 0.02Ca(OH)_2 \quad (3)$$

The works by Lamy et al.[39] and Liu et al.[40] showed that Ca_2SiO_4 exhibited very good bioactivity as plasma sprayed coating on Ti alloy substrates. Especially, as compared to γ-Ca_2SiO_4, β-Ca_2SiO_4 showed stronger hydration when it was soaked in SBF solution, and the hydration was favorable for the formation of a bone-like carbonate-containing hydroxyapatite (CHA) layer on the surface of the materials.[41,42] The TCP as one of the bioactive bone cements has also attracted increasing attention since the 1980s.[43] Ginebra et al.[44,45] have shown that the CDHA could be obtained in the manner of the following steps: (1) mixing α-TCP with a few HA as a cement powder,

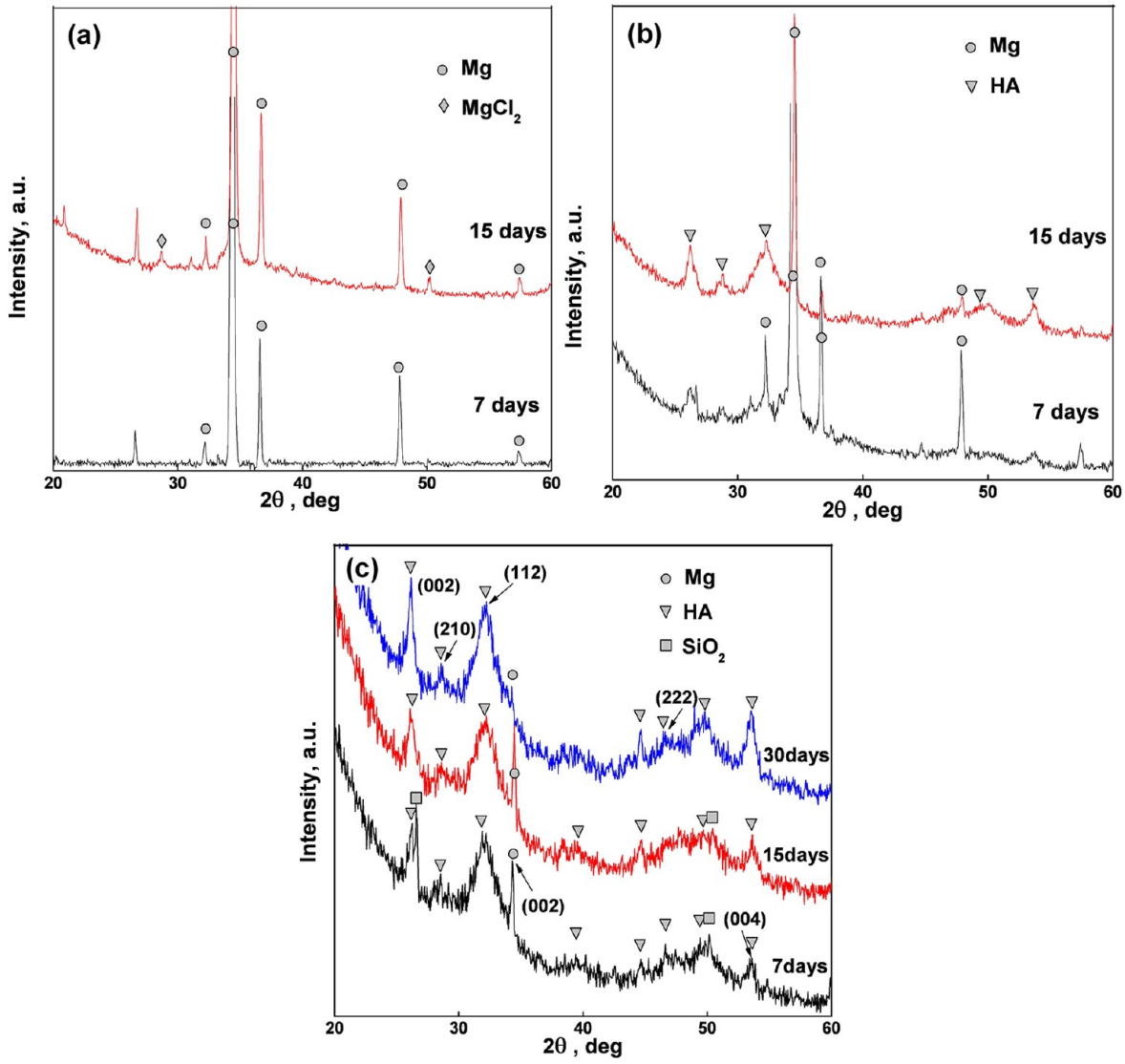

Figure 7. XRD spectra of the Mg with and without coatings soaked in SBF solution for different times. (a) Mg, (b) Ca–P coated Mg, and (c) BGCC/Ca–P coated Mg.

(2) mixing this powder with an aqueous solution of Na_2HPO_4 (as an accelerator) at a liquid-to-powder ratio of 0.32 mL/g, and (3) finally storing the mixed paste in Ringer's solution at either 22 or 37 °C for either 24 or 48 h. The reaction of the hydrolysis of α-TCP is as follows:

$$3Ca_3(PO_4) + H_2O \rightarrow Ca_9HPO_4(PO_4)_5OH(CDHA) \quad (4)$$

Durucan and Brown[46] and Monma and Kanazawa[47] also stated that the cement-type reaction occurred by hydrolysis and phase transition of α-TCP, leading to the formation of CDHA at low temperature. In the present work, XRD analysis implies that the Ca_2SiO_4 phase is probably the β-Ca_2SiO_4 phase, since all diffraction peaks of the Ca_2SiO_4 phase correspond to those of the typical β-Ca_2SiO_4 phase, and a few TCP exist in the Ca_2SiO_4 crystal as a solid solution state after heat-treatment at 800° C. From Figure 3b, it can be seen that the diffraction peaks of the BGC powders disappear completely, suggesting that the hydration reactions of the crystalline phases of BGC powders with H_2O occur, as indicated by eqs 3 and 4. Meanwhile, as the CaO phase, which is from the BG phase of BGC powders and the hydration products of Ca_2SiO_4, was immersed in phosphate solution, the following reaction occurs:

$$CaO + H_2O \rightarrow Ca^{2+} + OH^- \quad (5)$$

The pH value of the BGCC slurry was thus further increased, and this enhanced alkaline environment promotes the transformation of the hydrogen phosphate ion ($H_2PO_4^-$) and dihydrogen phosphate ion (HPO_4^{2-}) in the phosphate solution into PO_4^{3-} through the following ionic reactions:

$$H_2PO_4^- + OH^- \rightarrow HPO_4^{2-} + H_2O$$
$$HPO_4^- + OH^- \rightarrow PO_4^{2-} + H_2O \quad (6)$$

Then, the CDHA was produced by the reaction of Ca^{2+} with PO_4^{3-}:

$$9Ca^{2+} + 6PO_4^{3-} + H_2O \rightarrow Ca_9HPO_4(PO_4)_5OH(CDHA) \quad (7)$$

The BGC powders have higher specific surface area, so they have higher contact areas with phosphate solution, and the surface of the BGC powders was fully covered with CDHA as

dx.doi.org/10.1021/am404574t | ACS Appl. Mater. Interfaces 2014, 6, 513–525

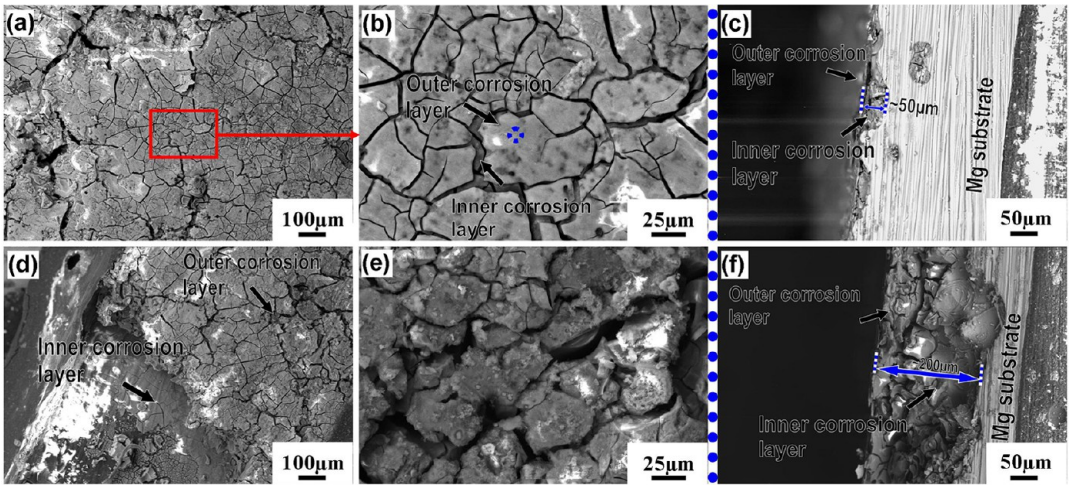

Figure 8. BSE images showing the surface morphologies and cross section of the pure Mg soaked in SBF solution for 7 day (a–c) and 15 days (d–f).

the reaction time was further prolonged. The CDHA forms not only on the surface of BGC powders, but also it exists among BGC powders (see Figure 6b,III), so that the BGCC slurry loses its liquidity and plasticity and becomes the solid BGCC coating after being dried at 50 °C for 24 h. Since it is very hard to "build a bridge" sufficiently among BGC powders by the newly formed CDHA crystals, the final structure exhibits a loose network morphology, as seen in Figure 4c.

(IV) When the Ca–P coated Mg was immersed in the BGCC slurry by the dipping–pulling method at RT, a certain amount of Ca^{2+} or PO_4^{3-} was released from the BGC powders or the surface layer of the primary Ca–P coating, respectively, and thus the new Ca–P composites were further deposited on the surface of the primary Ca–P coating, as seen in Figure 6b,II and b,IV.

3.3. Degradation of the Coating. Figure 7 shows the exterior phase of the Mg with and without coatings after immersion in SBF solution for different times. As shown in Figure 7a, the typical diffraction peaks of pure Mg appear in the XRD patterns of the Mg specimen immersed in SBF solution for 7 days. After a longer 15-day immersion, there are still no significant changes in the XRD patterns of pure Mg, but the diffraction peaks at $2\theta = 28.7°$ and 50.2° of the $MgCl_2$ phase have appeared, resulting from the corrosion of pure Mg by the chloride ions (Cl^-) from the SBF solution. For the Ca–P coated Mg, wide typical peaks of the HA phase appear (Figure 7b), indicating that the newly formed HA has a low degree of crystallization. In contrast, the typical peaks of HA have already appeared when the BGCC/Ca–P coated Mg was soaked in SBF solution for 7 days (Figure 7c), and the diffraction peaks of the HA become much sharper with increasing immersion time to 30 days, implying that the relative crystallinity of the HA was improved to some extent. This process could be explained by the fact that the CDHA on the surface of the BGCC coating reacted with the Ca^{2+} in SBF solution in an alkaline environment:

$$Ca_9HPO_4(PO_4)_5OH + Ca^{2+} + 2OH^- \rightarrow Ca_{10}(PO_4)_6(OH)_2 + H_2O \quad (8)$$

Furthermore, it is noted that the perpendicular direction to the HA crystal plane $(22\bar{4}2)$ disappears more quickly in comparison to the crystal planes (0002), $(21\bar{3}0)$, $(11\bar{2}2)$, and (0004), after immersion for 15 days, while it appears again after a longer 30-day immersion. This result indicates that the dissolution–precipitation reaction occurs on the crystal plane $(22\bar{4}2)$ during the HA crystal growth. Meanwhile, the relative intensity of the diffraction peak for the Mg crystal plane (0002) reduces gradually with increasing immersion time to 30 days (Figure 7c), which implies that the thickness of the newly formed HA deposition layer increases with increasing immersion time.

It should be pointed out here that, after immersion in SBF solution for 15 days, the pure Mg sample has been corroded rather seriously by the SBF solution, and the Ca–P coating of the Ca–P coated Mg sample has partially broken off from the sample surface. So the assessments of in vitro biominerization for the pure Mg and Ca–P coated Mg samples soaked in SBF solution for 30 days were not carried out in the present work.

3.4. In Vitro Mineralization. After the surface modification of Mg, if osteoconductive minerals could form on the surface of Mg at an early stage of degradation and the active coating still remains for the initial stage, the chances for achieving an osteointegrated interface would increase after implantation.[18]

To assess the in vitro biominerization of the Mg with and without Ca–P coating and BGCC/Ca–P coating, the specimens were soaked in SBF solution for different times, and the soaked surface morphologies and cross sections were then detected by SEM observations, as indicated in Figures 8–11.

The laminar corrosion layers including outer and inner corrosion layers were observed on the surface of the pure Mg after immersion in SBF solution for 7 days, as seen in Figure 8a, and there are a large number of corrosion cracks on the surface of the pure Mg. Some regions of the outer corrosion layer were corroded completely (Figure 8a), and a few of the Ca–P precipitates with a Ca/P molar ratio of approximately 1.00 were observed on the surface of the outer corrosion layer (Figure 8b); in this case, the total atomic volume of Ca and P on the surface of the inner corrosion layer are quite low, i.e., <6.0 atom %. Song et al.[21] observed the similar results on the surface of the pure Mg after immersion in SBF for a week, and they thought that the inner corrosion layer is probably composed of $Mg(OH)_2$ and $MgCO_3/Mg(HCO_3)_2$ phases. From the cross section of the pure Mg soaked in SBF solution for 7 days (Figure 8c), it can be clearly seen that the maximum thickness of the local corrosion layer is ~50 μm.

When the immersion time was prolonged to 15 days, the pure Mg was corroded seriously, leaving more cracks and holes,

dx.doi.org/10.1021/am404574t | ACS Appl. Mater. Interfaces 2014, 6, 513–525

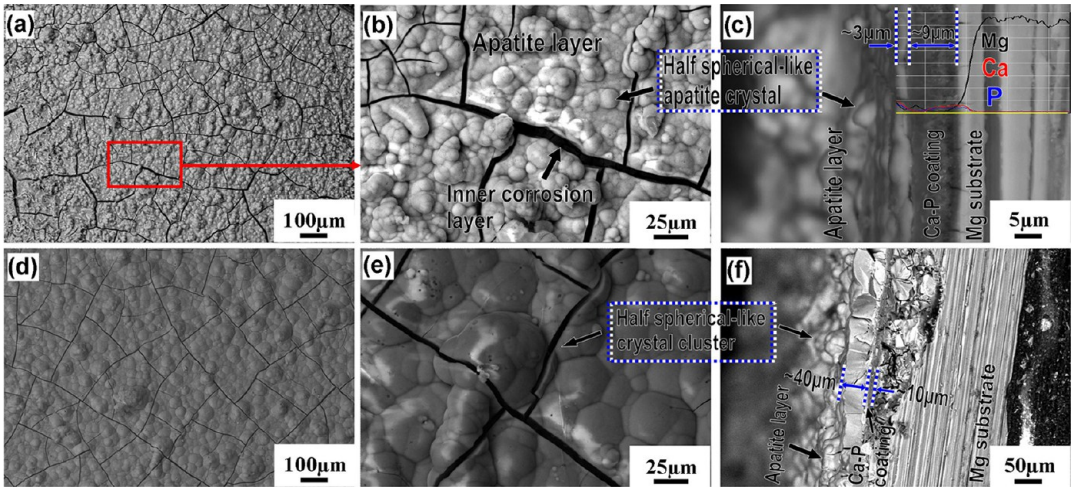

Figure 9. BSE images showing the surface morphologies and cross section of the Ca–P coated Mg soaked in SBF solution for 7 days (a–c) and 15 days (d–f) and corresponding distribution of Mg, Ca, and P on the section (c) of the Ca–P coated Mg. The line scan was performed along the yellow line in (c).

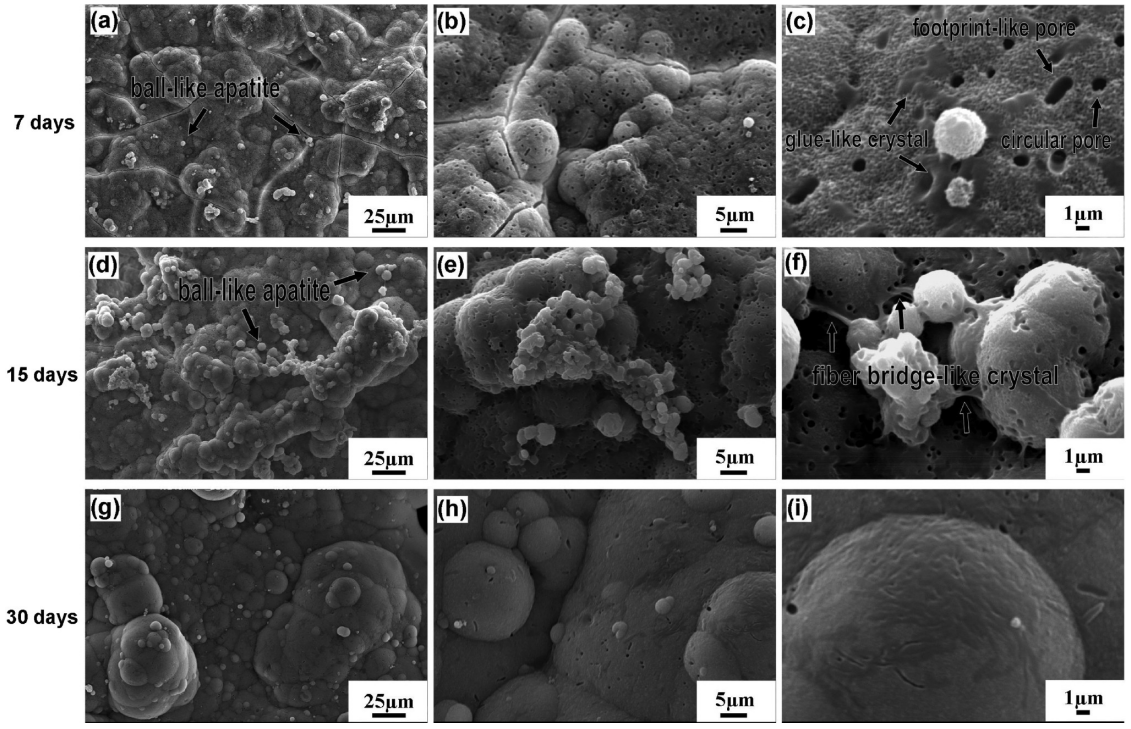

Figure 10. SEM images showing the surface morphologies of the BGCC/Ca–P coated Mg soaked in SBF solution for 7 days (a–c), 15 days (d–f), and 30 days (g–i).

and parts of the Mg substrate were corroded completely (Figure 8d). In a magnified image of Figure 8e, the outer corrosion layers were almost corroded by the SBF solution and the corrosion cracks of the inner corrosion layer further propagated. In this case, the thickness of the local corrosion layer increases to ~200 μm, as seen in Figure 8f, implying that the corrosion rate of Mg increases obviously.

Figure 9a,b shows the surface morphologies of the apatite layer deposited on the surface of Ca–P coated Mg immersed in SBF for 7 days. A thick deposition layer was observed on the surface of Ca–P coating as presented in Figure 9a. From a magnified image (Figure 9b), a number of irregular half sphere-like crystals with the diameter of about 10–20 μm formed on the top surface of the apatite deposition layer. EDS analysis indicates that the Ca/P molar ratio of these crystals varies from 1.26 to 1.91, which is higher than that of initial Ca–P coating (Ca/P = 0.78–1.10). The image of the cross section showing the distribution of Mg, Ca, and P of the Ca–P coated Mg soaked in SBF solution for 7 days is given in Figure 9c. Clearly, Ca and P elements were detected in the region of the Mg substrate, which is near the interface of Ca–P coating and Mg substrate, indicating that the interface of the Ca–P coating and Mg substrate sustains a certain stability after immersion in SBF solution for 7 days. The scan line profiles of Ca and P elements show a relatively broader peak in the region of the Ca–P coating with a thickness of ~9 μm. The scan line profiles of Ca

dx.doi.org/10.1021/am404574t | ACS Appl. Mater. Interfaces 2014, 6, 513–525

and P elements show relatively lower peaks, and the Mg element exhibits a high peak in the region of Ca−P coating, which is near the interface of Ca−P coating and apatite deposition layer. These results indicate that many Ca^{2+} and P^{5+} were released from the Ca−P coating into SBF solution, and an amount of Mg^{2+} from Mg substrate aggregated around the top surface of the Ca−P coating. Moreover, it can be seen that a thin apatite deposition layer with a thickness of ∼3 μm has formed on the surface of the Ca−P coating.

As the immersion time was prolonged to 15 days, a dense and uniform apatite deposition layer has been observed on the surface of Ca−P coating as presented in Figure 9d. In a magnified image (Figure 9e), it seems that the diameter of the irregular sphere-like crystals increases to about 25−75 μm. The cross section image of the Ca−P coated Mg soaked in SBF solution for 15 days is given in Figure 9f. Apparently, there is nearly no change in the thickness of Ca−P coating (∼10 μm), while the newly formed apatite deposition layer increases to ∼40 μm on the surface of the Ca−P coating. This phenomenon indicates that the Ca−P coating could keep stable in SBF solution and effectively induce the formation of apatite layer on its surface. However, it was found that the Ca−P coating in a few local areas has peeled from the surface of the Ca−P coated Mg after immersion in SBF solution for 7 days. With increasing immersion time to 15 days, the heavy breaking-off of the Ca−P coating has appeared on the surface of the Ca−P coated Mg, as seen in Figure 9f. This implies that the Mg substrate is corroded more seriously with increasing immersion time.

The SEM morphologies of the BGCC/Ca−P coated Mg after immersion in SBF solution for 7, 15, and 30 days are shown in Figure 10. After immersion in SBF for 7 days, those two kinds of particles as seen in Figure 4c cannot be observed completely on the surface of the BGCC coating, and a dense and thick deposition apatite crystal layer has formed on the surface of BGCC coating, with a few small ball-like crystals irregularly forming on the top surface of the apatite layer, as presented in Figure 10a. Actually, the deposition apatite layer is composed of many half ball-like crystals with the diameter of ∼5 μm (Figure 10 b), and the EDS results reveal that the Ca/P molar ratios of these half ball-like crystals vary from 1.23 to 1.3, which are quite close to the Ca/P molar ratio of OCP; thus OCP may be the main composition of these half sphere-like crystals, and it is considered as precursors of HA.[31] In a magnified image of Figure 10c, it is found that these half ball-like crystals are clusters comprising nano-sized fiber crystals, and a number of circular pores with ∼0.5 μm in size or footprint-like pores with ∼1 μm in size formed on the surface of the apatite layer. These pores can allow the fresh body fluid to be easily sent into the interior of the BGCC coating. Meanwhile, a few glue-like crystals also formed on the surface of the half ball-like crystals, and the Ca/P molar ratio of these glue-like crystals ranges from 1.64 to 1.70, which is close to that of HA; thus HA should be the main composition of these glue-like crystals. When the immersion time was prolonged to 15 days, the apatite deposition layer became denser and thicker, and an amount of ball-like crystal clusters with a Ca/P molar ratio of ∼1.5 formed on the apatite layer, as seen in Figure 10d,e, which is similar to the Ca/P molar ratio of TCP, so TCP might be the composition of these crystals. In a magnified image of Figure 10f, it is found that these ball-like crystal clusters are connected with apatite layer through some gluey bridge-like crystals, which are probably HA crystals.

After being immersed for 30 days, the density and thickness of the apatite deposition layer are clearly higher than in the case of 15 days, as shown in Figure 10g. The diameter of half ball-like crystal increases by several times. During the growth of half ball-like crystals, the crystal superposition phenomenon would occur, and finally a number of huge crystal clusters 50−125 μm in size form. Meanwhile, the circular pore size and density decrease on the surface of the apatite layer (see Figure 10h,i), and the glue-like crystals have not been found on the surface of the half ball-like crystals. The EDS analysis reveals that the Ca/P molar ratio of these half ball-like crystals varies from 1.45 to 1.56, which is also similar to the Ca/P molar ratio of TCP, so TCP might be the composition of these crystals. This result is almost the same with the case of 15 days. Thus, analysis of XRD (see Figure 7c) and EDS all proved that the newly formed apatite deposition layer consists mainly of HA, but a number of TCP crystals might be formed on the surface of the apatite deposition layer after immersion in SBF solution for 30 days.

The BSE image of the cross section showing the distribution of Mg, Ca, P, and Si of the BGCC/Ca−P coated Mg soaked in SBF solution for 30 days is given in Figure 11. It can be seen

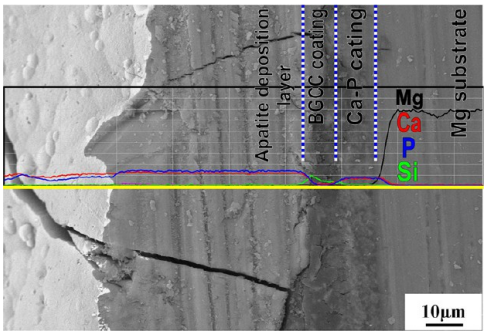

Figure 11. BSE image of the cross-section showing the distribution of Mg, Ca, P, and Si of the BGCC/Ca−P coated Mg soaked in SBF solution for 30 days. The line scan was performed along the yellow line.

that Ca and P elements were also detected in the region of the Mg substrate, which is near the interface of Ca−P coating and Mg substrate, indicating that the interface of the BGCC/Ca−P coating and Mg substrate still maintains a stability, to some extent, even after immersion in SBF solution for 30 days. The scan line profiles of Ca and P elements show a relatively broader peak in the region of Ca−P coating, and its thickness is still ∼10 μm. In contrast, most of BGCC coatings were corroded and the thickness of the BGCC coating thus greatly reduced down to ∼10 μm. The scan line profiles of Ca and P elements show relatively lower peaks in the region of BGCC coating, and the Si element exhibits a higher peak in the region of BGCC coating, which is near the interface of the BGCC coating and HA deposition layer. These results indicate that a good many Ca^{2+} and P^{5+} were released from the BGCC coating into the SBF solution, and an amount of silicon from the BG phase of BGCC were concentrated towards the top surface of the BGCC coating. In this case, a dense and uniform HA deposition layer with a thickness of ∼50 μm has formed on the surface of the BGCC coating. These experimental results strongly demonstrate that the BGCC/Ca−P coating prepared in the present work not only exhibits a good bone-like apatite layer induction activity and a bonding performance with the

Ca–P coated Mg substrate, but also it could greatly decrease the corrosion rate of the Mg substrate in SBF solution.

3.5. Biomineralization Mechanism of BGCC/Ca–P Coated Mg. Figure 12 shows the changes in Ca^{2+} and P^{5+}

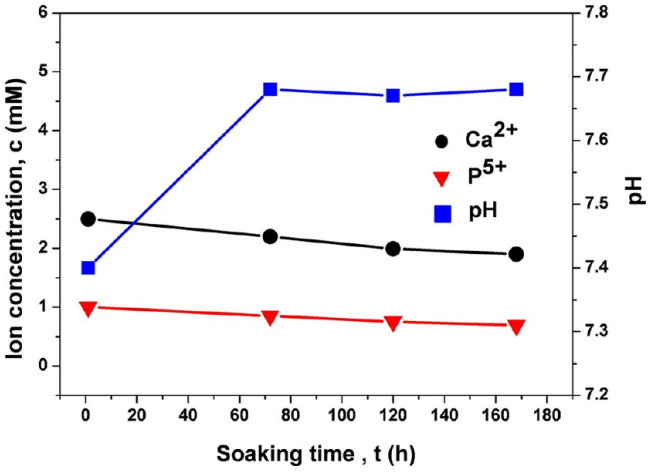

Figure 12. Changes in Ca^{2+} and P^{5+} concentrations and pH value of the BGCC/Ca–P coated Mg in SBF as a function of soaking time.

concentrations and pH value of the BGCC/Ca–P coated Mg immersed in SBF as a function of soaking time. In general, the concentrations of Ca^{2+} and P^{5+} of the SBF solution decrease slowly with the increase of immersion time, implying that the deposition rate of the apatite layer is higher than the dissolution rate of the Ca^{2+} and P^{5+} from the BGCC coating. The pH value of the SBF solution sharply increases in the first 72 h and then becomes almost constant. The reasons for the increase in pH value may be described as follows: (1) Mg ions are released from the Mg substrate into the solution and hydroxyl ions are produced (see eq 1), and (2) the CaO phase, which is from the BG phase of BGC powders and the hydration products of Ca_2SiO_4, reacts with H_2O to cause an increase in OH^- concentration (see eq 5) in the initial stage.

When the BGCC/Ca–P coated Mg was soaked in SBF solution, the apatite deposition layer, which is mainly composed of HA crystals with a defective structure, was formed on the surface of the BGCC coating, and the components and structural features of HA crystals are similar to those of the inorganic component of the nature bone, namely, HA. The formation mechanism of the apatite deposition layer on the surface of the BGCC/Ca–P coated Mg specimens could be explained as follows:

As the specimens were soaked in SBF, the CaO phase, which is from the BG phase of BGC powders and the hydration products of Ca_2SiO_4, will react continually with H_2O (see eq 5). Thus, the Ca^{2+} were concentrated in the interface of the SBF solution and BGCC coating, and the pH value of the SBF solution sharply increased in the initial stage. Then some of these Ca^{2+} rapidly reacted with CDHA (see eq 8) to form HA crystals; meanwhile, during the continued release of the Ca^{2+} and P^{5+} from BGCC coating into SBF solution, a large number of the silanol (Si–OH) groups formed in the surface layer of BGCC coating directly from SiO_2 or from the reactions of the BG phase of BGC powders and the hydration products of Ca_2SiO_4 with H_2O. The formation of Si–OH groups has an important effect on the nucleation and amount of HA.[48−51] Higher Ca^{2+} concentration can induce apatite formation on the surface of the specimens;[52] moreover, the other ions, like HPO_4^{2-}, CO_3^{2-}, etc., from the SBF solution would promote the formation of apatite nuclei. Once the nuclei were formed, the crystal will continuously grow up, because the SBF was oversaturated with respect to apatite, and finally the HA deposition layer was formed. In particular, a number of TCP crystals might be firstly formed on the surface of the apatite deposition layer and then transformed into HA crystals (see eqs 4 and 8), and the apatite deposition layer became more and more densified and thickened as the immersion time was further prolonged, as shown in Figure 13.

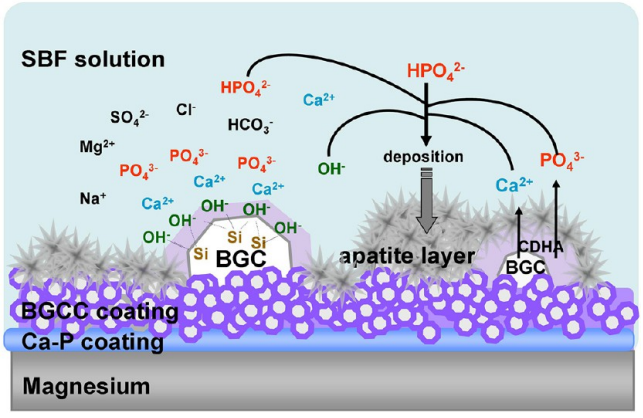

Figure 13. Schematic diagram of the formation of the apatite deposition layer on the surface of BGCC/Ca–P coated Mg in SBF solution.

3.6. Biocorrosion Performance of the Coating. In order to evaluate the protection capacity of Ca–P coating and BGCC/Ca–P coating to Mg substrate, the potentiodynamic polarization curves were obtained using an electrochemical workstation. Figure 14 shows the PDP curves of Mg substrate with and without Ca–P coating and BGCC/Ca–P coating in SBF at 37 °C. Values of the corrosion potential E_{corr} and the corrosion current i_{corr} were extracted from these curves, as given in Table 4.

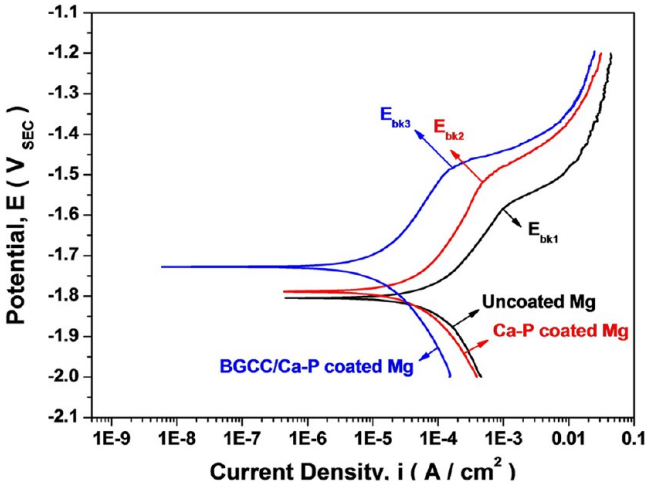

Figure 14. Potentiodynamic polarization curves of uncoated Mg, Ca–P coated Mg, and BGCC/Ca–P coated Mg tested in SBF solution at 37 °C.

dx.doi.org/10.1021/am404574t | ACS Appl. Mater. Interfaces 2014, 6, 513−525

Table 4. Electrochemical Parameters of Pure Mg, Ca−P Coated Mg, and BGCC/Ca−P Coated Mg

samples	corrosion potential E_{corr} (V)	corrosion current density i_{corr} (A/cm^2)
uncoated	−1.805	1.017×10^{-4}
Ca−P coated Mg	−1.789	4.799×10^{-5}
BGCC/Ca−P coated Mg	−1.728	1.291×10^{-5}

From results of PDP experiments, it can be obtained that the corrosion current density (i_{corr}) for the sample with BGCC/Ca−P coating is obviously lower than that of Ca−P coating and 10 times lower than that of uncoated Mg (see Table 4). Furthermore, a passivation region ranging from −1.76 V to −1.58 V is displayed in the PDP curve of pure Mg, indicating that a passive film is formed on the surface of Mg in SBF solution. With increasing anodic polarization potential, the coating is attacked at breakdown potential (E_{bk}); the coated Mg substrate suffers pitting corrosion. E_{bk2} (−1.51 V) of the Ca−P coated Mg is higher than E_{bk1}(−1.58 V) of the uncoated Mg, and E_{bk3} (−1.48 V) of the BGCC/Ca−P coated Mg is the highest. That means the corrosion resistance of Mg substrate could be effectively improved by Ca−P coating and especially by BGCC/Ca−P coating, primarily due to the fact that the coatings could decrease the available surface area susceptible to corrosion. The lowest corrosion current density was determined from the Tafel-type fit on the Mg with BGCC/Ca−P coating. Making comparisons with other results, it is known that the corrosion current density (i_{corr}) of BGCC/Ca−P coated Mg prepared by the present work (1.291×10^{-5} A/cm^2) is three times lower than that of DCPD and -TCP coated AZ91 alloy (3.650×10^{-5} A/cm^2) produced by the electrochemical deposition method[21] and 200 times lower than that of DCPD coated AZ91 alloy (2.600×10^{-3} A/cm^2) fabricated by the aqueous solution method[53] in SBF solution at 37 °C. These comparisons indicate that the BGCC/Ca−P coating could provide more efficient protection to the Mg substrate.

4. CONCLUSIONS

In order to improve the biocompatibility and osteointegration of pure Mg, two kinds of coatings, i.e., the Ca−P coating and BGCC/Ca−P coating, were prepared on the pure Mg ribbons in the present work. The following conclusions can be drawn:

(1) The Ca−P coating was firstly produced by aqueous solution method. Subsequently, Ca−P coated Mg was immersed into the BGCC slurry with a liquid-to-solid ratio (L/S) of 1.6 to obtain BGCC/Ca−P coating by a dipping−pulling method. The results of EDS and XRD show that the Ca−P coating consists mainly of Ca−P composites with the Ca/P molar ratio lower than 1, and the BGCC coating consists mainly of CDHA.

(2) The in vitro bioactivity assessments show that the mineralization ability of the Ca−P coated Mg and BGCC/Ca−P coated Mg are significantly better than that of pure Mg. After the specimens were immersed in SBF solution for 7 days, the bone-like apatite layer consisting of half spherical crystal clusters has deposited on the surface of the Ca−P coating and BGCC/Ca−P coating; as the immersion time was prolonged to 15 days, the Ca−P coating could still keep stable in SBF solution and induce the formation of apatite deposition layer on its surface. When the immersion time is prolonged to 30 days, a dense HA layer with the thickness of ∼50 μm has deposited on the surface of the BGCC/Ca−P coated Mg.

(3) The corrosion current density obtained from the potentiodynamic polarization curves for the BGCC/Ca−P coated Mg is obviously lower than that of Ca−P coating and 10 times lower than that of uncoated Mg. The BGCC/Ca−P coating can significantly decrease the degradation rate of Mg and introduce a high biocompatibility of the bone−Mg substrate interface. In summary, BGCC/Ca−P coated Mg has a good potential for biomedical applications.

AUTHOR INFORMATION

Corresponding Author

*(X.-W.L.) Tel.: +86 24 83678479. E-mail: xwli@mail.neu.edu.cn.

Notes

The authors declare no competing financial interest.

ACKNOWLEDGMENTS

This work was financially supported by the Fundamental Research Funds for the Central University of China under Grants N110605003, N110105001, and N120505001 and partially by the National Natural Science Foundation of China (NSFC) under Grants 51231002 and 51271054. X.-W.L. is grateful for this support.

REFERENCES

(1) Witte, F.; Kaese, V.; Haferkamp, H.; Switzer, E.; Meyer-Lindenberg, A.; Wirth, C. J.; Windhagen, H. *Biomaterials* **2005**, *26*, 3557−3563.

(2) Witte, F.; Fischer, J.; Nellesen, J.; Crostack, H.-A.; Kaese, V.; Pisch, A.; Beckmann, F.; Windhagen, H. *Biomaterials* **2006**, *27*, 1013−1018.

(3) Xu, L.; Yu, G.; Zhang, E.; Pan, F.; Yang, K. *J. Biomed. Mater. Res. A* **2007**, *83A*, 703−711.

(4) Serre, C.; Papillard, M.; Chavassieux, P.; Voegel, J. C.; Boivin, G. *J. Biomed. Mater. Res.* **1998**, *42*, 626−633.

(5) Zhang, X.; Li, X. W.; Li, J. G.; Sun, X. D. *Prog. Nat. Sci.: Mater. Int.* **2013**, *23*, 183−189.

(6) Staiger, M. P.; Pietak, A. M.; Huadmai, J.; Dias, G. *Biomaterials* **2006**, *27*, 1728−1734.

(7) Song, G. *Corros. Sci.* **2007**, *49*, 1696−1701.

(8) Yin, D.; Zhang, E.; Zeng, S. *Trans. Nonferrous Met. Soc. China* **2008**, *18*, 763−768.

(9) Zhang, E.; Yin, D.; Xu, L. P.; Yang, L.; Yang, K. *Mater. Sci. Eng. C* **2009**, *29*, 987−993.

(10) Xu, L. P.; Zhang, E. L.; Yin, D.; Zeng, S.; Yang, K. *J. Mater. Sci.: Mater. Med.* **2008**, *19*, 1017−1025.

(11) Zhang, E.; Xu, L.; Yu, G.; Pan, F.; Yang, K. *J. Biomed. Mater. Res.* **2009**, *90A*, 882−893.

(12) Wan, Y.; Xiong, G.; Luo, H.; He, F.; Huang, Y.; Zhou, X. *Mater. Des.* **2008**, *29*, 2034−2037.

(13) Li, Z.; Gu, X.; Lou, S.; Zheng, Y. *Biomaterials* **2008**, *29*, 1329−1344.

(14) Kim, W. C.; Kim, J. G.; Lee, J. Y.; Seok, H. K. *Mater. Lett.* **2008**, *62*, 4146−4148.

(15) Cui, F. Z.; Yang, J. X.; Jiao, Y. P.; Yin, Q. S.; Zhang, Y.; Lee, I. S. *Front. Mater. Sci. China* **2008**, *2*, 143−148.

(16) Hiromoto, S.; Yamamoto, A. *Electrochim. Acta* **2009**, *54*, 7085−7093.

(17) Xu, L. P.; Zhang, E. L.; Yang, K. *J. Mater. Sci.: Mater. Med.* **2009**, *20*, 859−867.

(18) Xu, L. P.; Pan, F.; Yu, G. N.; Yang, L.; Zhang, E. L.; Yang, K. *Biomaterials* **2009**, *30*, 1512−1523.

(19) Chen, X. B.; Birbilis, N.; Abbott, T. B. *Corros. Sci.* **2011**, *53*, 2263−2268.

(20) Chen, X. B.; Birbilis, N.; Abbott, T. B. *Corrosion* **2011**, *67*, 035005-1−035005-16.
(21) Song, Y. W.; Shan, D. Y.; Han, E. H. *Mater. Lett.* **2008**, *62*, 3276−3279.
(22) Wen, C. L.; Guan, S. K.; Peng, L.; Ren, C.X.; Wang, X.; Hu, Z. H. *Appl. Surf. Sci.* **2009**, *255*, 6433−6438.
(23) Meng, E. C.; Guan, S. K.; Wang, H. X.; Wang, L. G.; Zhu, S.J.; Hu, J.H.; Ren, C. X.; Gao, J. H.; Feng, Y. S. *Appl. Surf. Sci.* **2011**, *257*, 4811−4816.
(24) Song, Y.; Zhang, S. X.; Li, J. N.; Zhao, C. L.; Zhang, X. N. *Acta Biomater.* **2010**, *6*, 1736−1742.
(25) Wang, Y. M.; Wang, F. H.; Xu, M. J.; Zhao, B.; Guo, L. X.; Ouyang, J. H. *Appl. Surf. Sci.* **2009**, *255*, 9124−9131.
(26) Wu, C.; Wen, Z.; Dai, C.; Lu, Y.; Yang, F. *Surf. Coat. Technol.* **2010**, *204*, 3336−3347.
(27) Liu, G. Y.; Hu, J.; Ding, Z. K.; Wang, C. *Appl. Surf. Sci.* **2011**, *257*, 2051−2057.
(28) Tang, H.; Yu, D. Z.; Lou, Y.; Wang, F. P. *Appl. Surf. Sci.* **2013**, *264*, 816−822.
(29) Kokubo, T.; Yoshihara, S.; Nishimura, N.; Yamamuro, T.; Nakamura, T. *J. Am. Ceram. Soc.* **1991**, *74*, 1739−1741.
(30) Kokubo, T.; Kushitani, H.; Sakka, S.; Kitsugi, T.; Yamamuro, T. *J. Biomed. Mater. Res.* **1990**, *24*, 721−734.
(31) Fu, Q.; Zhou, N.; Huang, W. H.; Wang, D. P.; Zhang, L. Y. *J. Chin. Ceram. Soc.* **2004**, *32*, 901−905.
(32) Liu, J. X.; Gao, S. S.; Shi, F.; Wang, Z. Y.; Zhang, G. X.; Xu, L. Q. *J. Chin. Ceram. Soc.* **2009**, *37*, 441−446.
(33) Zhang, J. M.; Lin, C. J.; Feng, Z. D.; Tian, Z. W. *J. Electroanal. Chem.* **1998**, *452*, 235−240.
(34) Dumlie, N.; Benhayoune, H.; Richard, D.; Laurent-Maquin, D.; Balossier, G. *Mater. Charact.* **2006**, *59*, 129−133.
(35) Fadeev, I. V.; Shvorneva, L. I.; Barinov, S. M.; Orlovskii, V. P. *Inorg. Mater.* **2003**, *39*, 947−950.
(36) Ishida, H.; Okada, Y.; Mitsuda, T. *J. Am. Ceram. Soc.* **1992**, *75*, 359−363.
(37) Ishida, H.; Sasaki, K.; Mitsuda, T.; Okada, Y.; Mitsuda, T. *J. Am. Ceram. Soc.* **1992**, *72*, 2779−2784.
(38) Fujii, K.; Konda, W. *J. Am. Ceram. Soc.* **1979**, *62*, 161−167.
(39) Lamy, D.; Pierrc, A. C.; Heimann, R. B. *J. Mater. Res.* **1996**, *11*, 680−686.
(40) Liu, X. Y.; Tao, S. Y.; Ding, C. X. *Biomaterials* **2002**, *23*, 963−968.
(41) Gou, Z.; Chang, J. *J. Eur. Ceram. Soc.* **2004**, *24*, 93−99.
(42) Gou, Z. R.; Chang, J.; Zhai, W. Y.; Wang, J. Y. *J. Biomed. Mater. Res. B* **2005**, *73*, 244−251.
(43) Chow, L. C. *J. Ceram. Soc. Jpn.* **1991**, *99*, 954−964 (The Centennial Memorial Issue).
(44) Ginebra, M. P.; Fernandez, E.; Driessens, F. C. M.; Boltong, M. G.; Muntasell, J.; Font, J.; Planell, J. A. *J. Mater. Sci.: Mater. Med.* **1995**, *6*, 857−860.
(45) Ginebra, M. P.; Fernandez, E. F.; De Maeyer, E. A. P.; Verbeeck, R. M. H.; Boltong, M. G.; Ginebra, J.; Driessens, F. C. M.; Plane, J. A. *J. Dent. Res.* **1997**, *76*, 905−912.
(46) Durucan, C.; Brown, P. W. *J. Mater. Sci.: Mater. Med.* **2000**, *11*, 365−371.
(47) Monma, H.; Kanazawa, T. *J. Ceram. Soc. Jpn.* **2000**, *108*, 75−80.
(48) Hench, L. L. *Bioceramics* **1994**, *7*, 3−13.
(49) Li, P.; Ohtsuki, C.; Kokubo, T.; Nakanishi, K.; Soga, N.; Nakamura, T.; Yamamuro, T. *J. Am. Ceram. Soc.* **1992**, *75*, 2094−2097.
(50) Li, X. W.; Yasuda, H. Y.; Umakoshi, Y. *J. Mater. Sci.: Mater. Med.* **2006**, *17*, 573−581.
(51) Zhang, X.; Xiu, Z. M.; Li, X. W. *Adv. Mater. Res.* **2011**, *217-218*, 88−92.
(52) Kokubo, T.; Takadama, H. *Biomaterials* **2006**, *27*, 2907−2915.
(53) Hu, J.; Wang, C.; Ren, W. C.; Zhang, S.; Liu, F. *Mater. Chem. Phys.* **2010**, *119*, 294−298.